# A Novel Mechanism by Which Small Molecule Inhibitors Induce the DFG Flip in Aurora A

Mathew P. Martin, Jin-Yi Zhu, Harshani R. Lawrence, Roberta Pireddu, Yunting Luo, Riazul Alam, Sevil Ozcan, Said M. Sebti, Nicholas J. Lawrence, and Ernst Schönbrunn*

Drug Discovery Department, Moffitt Cancer Center and Research Institute, 12902 Magnolia Drive, Tampa, Florida 33612, United States

S *Supporting Information*

ABSTRACT: Most protein kinases share a DFG (Asp-Phe-Gly) motif in the ATP site that can assume two distinct conformations, the active DFG-in and the inactive DFG-out states. Small molecule inhibitors able to induce the DFG-out state have received considerable attention in kinase drug discovery. Using a typical DFG-in inhibitor scaffold of Aurora A, a kinase involved in the regulation of cell division, we found that halogen and nitrile substituents directed at the N-terminally flanking residue Ala273 induced global conformational changes in the enzyme, leading to DFG-out inhibitors that are among the most potent Aurora A inhibitors reported to date. The data suggest an unprecedented mechanism of action, in which induced-dipole forces along the Ala273 side chain alter the charge distribution of the DFG backbone, allowing the DFG to unwind. As the ADFG sequence and three-dimensional structure is highly conserved, DFG-out inhibitors of other kinases may be designed by specifically targeting the flanking alanine residue with electric dipoles.

R = F, Cl, Br, CN

DFG-in → DFG-out

GLY276 PHE275 ALA273 ASP274
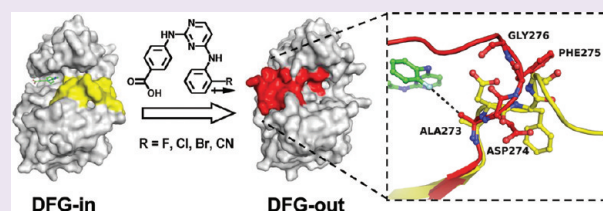
Recent successes in the development of small molecule protein kinase inhibitors as drugs have led to an influx in kinase-directed drug discovery programs.[1] The Aurora kinase family constitutes one class of serine/threonine protein kinases that are located in the nucleus and are fundamentally involved in the regulation of cell division.[2,3] The three Aurora isoforms, A, B, and C, differ in substrate specificity and function. Aurora A plays a regulatory role in chromosome maturation and mitotic spindle assembly and is activated by the microtubule-associated protein TPX2.[4] Aurora B subsequently acts in chromosomal segregation and cytokinesis and is regulated by inner centromeric protein (INCENP), a subunit of the chromosomal passenger complex.[5] Although Aurora C is known to be expressed in germ cells, its function remains elusive.

Expression levels of Aurora A and B kinases are upregulated in many human cancers, including colorectal, breast, and ovarian.[6] Therefore, the Aurora kinase family has received attention as a target for the development of anticancer therapeutics.[7] One such compound, VX680, was identified as a potent pan-Aurora inhibitor with inhibition constant (K_i) values of 0.6, 18, and 4.6 nM against Aurora A, B, and C, respectively;[8] however, clinical trials were halted due to serious cardiac events.[9] Other Aurora inhibitors have since been developed, including AT9283[10] and MLN8237[11] which are currently in clinical trials (www.clinicaltrials.gov).

A majority of protein kinases share a common DFG (Asp-Phe-Gly) motif in the ATP site that transitions between two distinct conformations in response to phosphorylation of the contiguous activation loop: the active DFG-in and the inactive

DFG-out states. Kinase inhibitors that bind only to the DFG-in state often suffer from a lack of target specificity, as the ATP site is wide open and able to accommodate diverse chemical scaffolds. By contrast, inhibitors able to induce and stabilize the DFG-out conformation are considered superior, as they render the active site architecture incompatible with substrate binding, resulting in enhanced potency and target selectivity. The clinical success of imatinib (Gleevec) as an inhibitor of Abl kinase[12] is attributed in large part to this distinct mode of action[13] and has spurred the design of DFG-out inhibitors for other kinases, including MAP,[14] JNK2,[15] Nek2,[16] and Eph receptor tyrosine kinase.[17] However, all known Aurora kinase inhibitors, such as the aforementioned chemical probe VX680, are DFG-in inhibitors. Although the DFG motif is highly conserved among protein kinases, the mechanism by which small molecules induce the DFG flip is not well understood. Small molecules able to induce large conformational changes in the target enzyme have potential as superior lead compounds in drug discovery, as the altered structure of the dead-end complex is less suited for efficient interaction with substrate. This concept has led to the design of some of the most clinically successful kinase inhibitors to date. Imatinib and sorafenib stabilize the DFG-out conformation by establishing a bridging network of hydrogen bonds between the amide/urea inhibitor core and both a conserved glutamate side chain within the C-helix and the main chain amide of the DFG aspartate residue.[18]
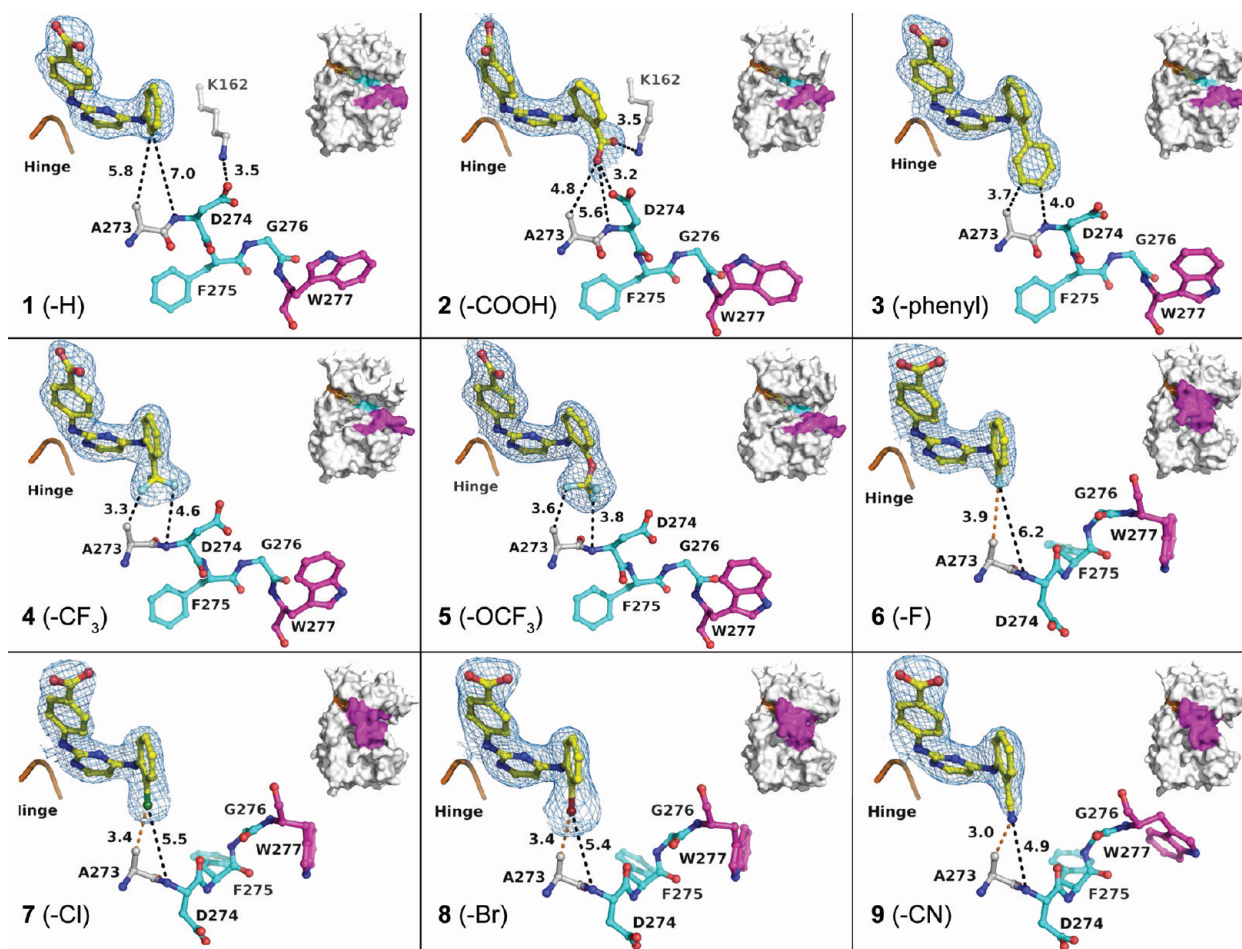
Figure 1. Binding modes of bisanilinopyrimidine inhibitors with Aurora A. Crystal structures were determined for Aurora A liganded with different *ortho*-substituted bisanilinopyrimidine inhibitors (Supplementary Tables 1 and 2). The hinge region (residues 211−213) is indicated in orange, the DFG (residues 274−276) in cyan, the activation loop (residues 277−293) in magenta, other residues in gray, and the inhibitor in yellow. The dotted lines indicate the closest distances to the DFG. The $2F_o - F_c$ electron density, contoured at 1 σ, is shown as blue mesh around the inhibitor; the $F_o - F_c$ electron density maps from refinements omitting the inhibitor are shown in the Supporting Information (Supplementary Figure 5). The insets in the top right corners are surface representations of the overall structures. Compounds **1−5** are DFG-in inhibitors; compounds **6−9** are DFG-out inhibitors.
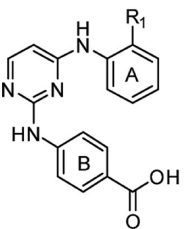
Molecular dynamics simulations were used to elucidate and propose a mechanism for the DFG-out conformation in MAPK p38α, in which the phenylalanine of the DFG motif is forced by the inhibitor from its hydrophobic pocket in the DFG-in (active state) to the solvent-exposed DFG-out (inactive state),[19] triggering an overall rearrangement of the activation loop. However, the knowledge gained from these structures did not translate into an applicable method for the rational design of DFG-out inhibitors of other kinases.

In an attempt to design DFG-out inhibitors of Aurora A, we utilized a bisanilinopyrimidine scaffold, recently discovered by high-throughput screening (HTS) to be a potent DFG-in inhibitor of this enzyme (Lawrence *et al.*, submitted). A series of co-crystal structures established that electronegative and electron-withdrawing substituents, directed at the N-terminally flanking residue Ala273, yielded highly potent DFG-out inhibitors able to induce and stabilize a unique "DFG-out/loop-in" conformation. The data suggest an unprecedented mechanism of action, by which induced-dipole forces disrupt the charge distribution along the DFG peptide, causing the DFG to unwind. As the ADFG sequence is highly conserved among kinases, the strategy employed here to inhibit Aurora A may be applicable to other kinases as well.

■ RESULTS AND DISCUSSION

Selection of a Chemical Scaffold Suitable To Probe the DFG Motif of Aurora A. We recently discovered compound **2** by HTS as a potent inhibitor of Aurora A with an IC_{50} value of 6.1 nM *in vitro* (Lawrence *et al.*, submitted). The co-crystal structure confirmed that **2** is a typical Type I inhibitor that binds to the hinge region (Ala213) without perturbing the DFG-in state (Asp274-Phe275-Gly276) (Figure 1, Table 1). The unusually high potency of the hit compound, the feasibility of focused library synthesis of the bisanilinopyrimidine scaffold, and the availability of robust co-crystallization conditions prompted us to probe the DFG region of Aurora A for the design of DFG-out inhibitors. We explored the *ortho*-position of the A-ring, as it is appropriately positioned for the introduction of functional groups to target the DFG. Synthesized analogues were characterized by enzyme kinetics, isothermal titration calorimetry (ITC), and protein crystallography. Inhibitory activity (expressed as IC_{50}) and binding affinity (expressed as dissociation constant, K_d) followed the same trend among the substituents tested (Figure 1, Table 1). The consistently higher K_d values obtained by ITC are likely due to differences in experimental conditions and detection

Table 1. Inhibitory Activity and Binding Affinity of Bisanilinopyrimidine Inhibitors Towards Aurora A

Cmpd	PDB	R_1	IC_{50} (nM)[a]	ITC[a] K_d (nM)	ITC[a] ΔH (kcal mol^{-1})	ITC[a] $T\Delta S$ (kcal mol^{-1})
1	3UO5	-H	10 ± 1.6	39 ± 5.9	−14	−3.9
2	3UP7	-COOH	6.1 ± 1.0	34 ± 5.9	-14	−3.4
3	3UO4	-phenyl	149 ± 23	299 ± 27	−3.0	5.6
4	3UOD	-CF$_3$	35 ± 4.1	49 ± 5.2	−14	−4.2
5	3UP2	-OCF$_3$	28 ± 4.8	40 ± 5.6	−11	−1.2
6	3UNZ	-F	3.7 ± 0.7	16 ± 1.6	−17	−6.1
7	3UO6	-Cl	2.5 ± 0.3	15 ± 1.5	−17	−6.3
8	3UOH	-Br	2.1 ± 0.4	13 ± 2.2	−15	−4.1
9	3U0J	-CN	43 ± 8.0	51 ± 5.5	−16	−6.2
VX680			2.8 ± 0.3	17 ± 3.7	−12	−2.1

[a]Experimental data are shown in the Supplementary Figures 1 and 2.

limits of the activity and binding assays (see Methods). Compounds **7**, **8**, and **10** were equal to or more potent than the well-studied Aurora inhibitor VX680, which displayed an IC_{50} value of 2.8 nM. For comparison, the *in vitro* activity of VX680 against Aurora A was previously determined to IC_{50} = 1.4 nM[10] and K_i = 0.6 nM[8] using different assays.

Halogen Substituents Induce a DFG-out State with Concomitant Closure of the ATP Site. The major difference between the binding interactions of hit compound **2** and all other compounds tested is the establishment of a salt bridge between the carboxyl group on the A-ring and the side chain of Lys162 (Figure 1, Supplementary Figure 3). Lys162 normally interacts with the carboxyl group of Asp274, and the loss of Lys162 as a binding partner allows the Asp274 side chain to swing toward the inhibitor (Lawrence, et al., submitted). A similar interaction pattern is found upon binding of ADP, in which the diphospho moiety interacts with both Lys162 and Asp274. The unsubstituted parent compound **1** retains high activity and binding affinity as fewer spatial constraints and loss of the electrostatic interaction with Lys162 allow the A-ring to rotate by approximately 40° into a position that is presumably more energetically favorable. Introducing a phenyl group (**3**) resulted in significant reduction of activity due to steric hindrance with the DFG segment. Although the DFG segment shifts away from the inhibitor to accommodate the bulky phenyl ring, the DFG-in state is maintained. In addition, the A-ring rotates away from the favorable orientation of **1**. The trifluoromethyl (**4**) and trifluoromethoxy (**5**) substituents were approximately 3-fold less active than parent compound **1**. These substituents caused steric hindrance with the DFG as indicated by rotation of the A-ring, particularly for **5**. Binding of **4** and **5** induced a flip of the Ala-Asp peptide bond from a *cis*-like configuration to *trans*. This backbone structural change is localized and did not alter the DFG-in conformation, but it indicated that the N-terminal flank of the DFG may respond to halogen substituents.

Remarkably, introduction of a fluorine (**6**), chlorine (**7**), or bromine (**8**) moiety resulted in a significant increase of inhibitory activity and binding affinity for progressively larger

and less electronegative substituents (Table 1). Co-crystallization attempts using the established conditions for DFG-in inhibitors **1−5** were unsuccessful, and in-diffusion experiments using crystals of ligand-free Aurora A resulted in rapid deterioration of diffraction power. These observations suggested that compounds **6−8** induce structural changes in the enzyme that are incompatible with the crystal lattice. We therefore established new conditions suitable for the crystallization of Aurora A in the presence of these inhibitors. The resulting structures revealed a complete switch from the DFG-in to the DFG-out state (Figures 1 and 2). In the DFG-out state, Asp274 is rotated approximately 100° away from the ATP site and interacts with Arg255 and Asn256 (Figure 2). The main chain conformational change of Asp274 is perpetuated toward Phe275 and Gly276, resulting in a complete 180° flip of the DFG motif and the adjacent activation loop (residues 277−293), which moves inward atop the ATP cleft. The new loop conformation is stabilized by hydrogen bonding interactions between the main chain atoms of Lys141 and His280. As a result of the DFG flip, Trp277 shifts position from a largely polar environment to a strictly hydrophobic pocket providing additional stability to the new loop conformation (Figure 2c and Supplementary Figure 8). Another effect of the DFG flip is a ∼4 Å shift in the C-helix and movement of the catalytic glutamate residue (Glu181) away from the ATP active site to accommodate the new conformation of Phe275. The closed loop conformation exhibits clearly defined electron density for the N-terminal strand (residues 277−282), which is antiparallel to a *β*-strand of the upper N-terminal lobe of the kinase domain. In contrast, the tip of the loop (residues 283−289) is largely flexible (Figure 2d). Notably, VX680 and compound **1** share the same DFG-in mode of action with similar conformations of the DFG segment and the activation loop (Figure 2e).

The high potency of the halogenated compounds **6−8** appears to result from structural rearrangement of the activation loop, which effectively shields the inhibitor from solvent and ATP in the dead-end complex. The increase in enthalpy observed by ITC (Table 1) is likely due to the
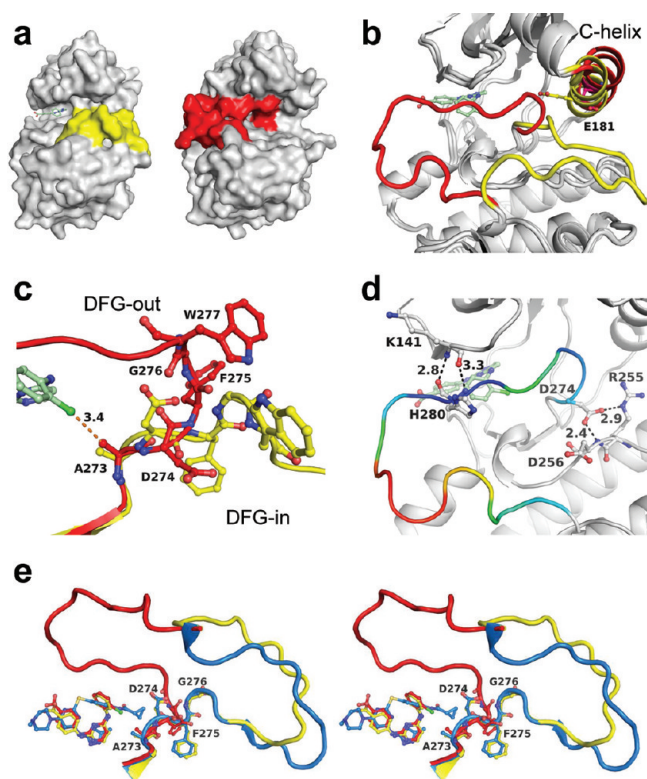
Figure 2. Structural changes in Aurora A induced by DFG-out inhibitors. (a) Surface representation of Aurora A in the DFG-in state (left, liganded with **1**) and DFG-out state (right, liganded with **7**); the activation loop is highlighted in yellow and red, respectively, and the inhibitors are shown in green. (b) Superposition reveals global conformational changes upon binding of **7** particularly of the activation loop and the C-helix, which harbors the catalytic residue Glu181. In the DFG-in state, the loop is oriented away from the ATP site and the inhibitor is exposed to solvent. In the DFG-out state, the loop flips by ~180° and the N-terminal flank is positioned above the active site, shielding the inhibitor from solvent. (c) Conformation of the ADFGW segment in the DFG-in state liganded with **1** (yellow) and the DFG-out state liganded with **7** (red). The residue closest to the inhibitor is Ala273 (3.4 Å). The DFG-flip causes drastic conformational changes of the backbone, beginning with residue Asp274, forcing Trp277 and the entire activation loop to change direction. The binding interactions of Trp277 in the DFG-in and DFG-out states are shown in Supplementary Figure 8. The C-helix of panel b gives way to accommodate the new conformation of Phe275. (d) In the DFG-out conformation, the side chain of Asp274 interacts with residues Arg255 and Asp256, and the conformation of the activation loop is stabilized through hydrogen bonding interactions between the main chain atoms of His280 and Lys141. The loop is colored according to temperature factors from blue (low B-factor) to red (high B-factor). Potential hydrogen bonding interactions are indicated as black dotted lines. (e) Comparison of the molecular mode of action of VX680 (blue, PDB 3E5A), compound **1** (yellow), and compound **7** (red) (stereo presentation).

addition of hydrogen bonding interactions between the loop and the enzyme upon inhibitor binding. We further probed the chlorinated scaffold of **7** by introducing a fluorine in the pyrimidine ring (**10**), which increased the inhibitory potency by greater than 2-fold (IC$_{50}$ = 0.8 nM). The co-crystal structure confirmed the DFG-out mode of **10** and the increased potency over **7** is attributable to additional van der Waals interactions of the fluorine substituent with the small hydrophobic pocket around the gatekeeper residue Leu210 (Figure 3). Substitution
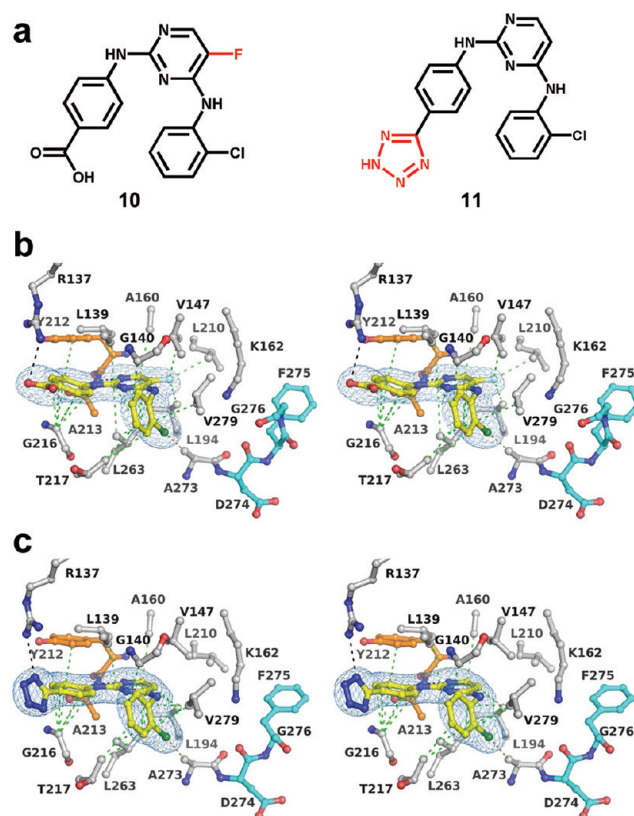
Figure 3. Substitutions in other regions of the bisanilinopyrimidine scaffold do not affect the DFG-out mode of action (stereo presentations). (a) Compounds **10** and **11** are analogues of the DFG-out inhibitor **7** (substitutions are highlighted in red). Both inhibitors induced the DFG flip and displayed the same general interaction pattern as **7**. (b) Introduction of a fluorine to the pyrimidine ring (**10**) fosters van der Waals interactions with hydrophobic residues around the gatekeeper residue Leu210, resulting in increased inhibitory activity. (c) Substitution of tetrazole for carboxyl in the *para*-position of the B-ring (**11**) preserves the electrostatic interaction with Arg137, and the inhibitory potency remains unchanged. Shown in blue mesh is the $2F_o - F_c$ electron density of the inhibitors, contoured at 1 σ. Potential hydrogen bonding and hydrophobic interactions are indicated as black and green dotted lines, respectively.

of the *p*-carboxyl group of the B-ring with a tetrazole moiety (**11**) rendered the DFG-out characteristics unchanged but did not improve inhibitory activity (IC$_{50}$ = 3.1 nM). The tetrazole ring mimics the anionic character of the carboxyl group by establishing a salt bridge with Arg137. The data demonstrate that substitutions in other regions of the bisanilinopyrimidine scaffold do not affect the DFG-out mode of action of *ortho* substituents in the A-ring.

DFG-out Inhibitors Target Ala273, the Residue N-terminal to the DFG. As we probed only the *ortho* position of the B-ring, the observed conformational changes must be solely attributed to the substituents in this position. Analysis of the binding interactions of monohalogenated inhibitors **6**, **7**, and **8** in the respective dead-end complexes did not reveal an obvious reason for the unique conformational changes of the DFG and the activation loop. The position of the A-ring remains unchanged with respect to parent compound **1**, and no additional interactions with enzyme residues are observed at first glance. The DFG flip cannot be attributed to steric forces, as the bulky phenyl and trifluoromethoxy substituents of **3** and
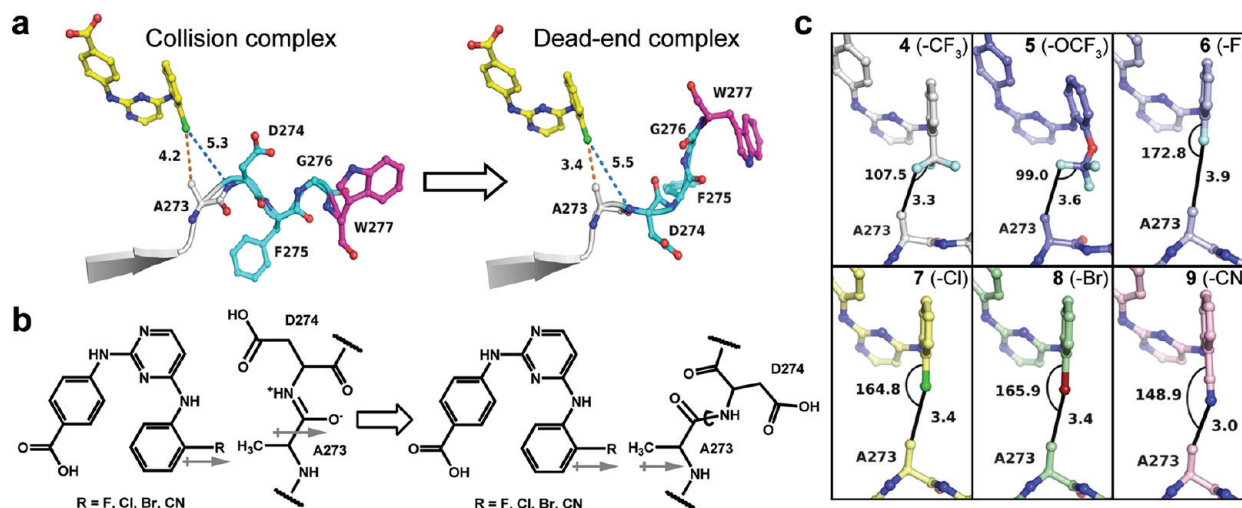
Figure 4. Proposed dipole-induced mechanism of action for Aurora ADFG-out inhibitors. a) Model of the collision complex of the DFG-in state of Aurora A with the DFG-out inhibitor **7**, based on superimposition of the co-crystal structures of **7** and **1**. Displayed are the closest distances (Å) between the chlorine substituent and the enzyme. The ~0.8 Å reduced distance in the dead-end complex indicates attraction of Ala273, a feature observed for the DFG-out inhibitors **6**–**9** and, to a lesser degree, for the DFG-in inhibitors **4** and **5** (Supplementary Figures 3 and 4). (b) The electric dipoles along the C–R bonds (R = F, Cl, Br, C≡N) of the inhibitor may induce a dipole along the C_α–C_β bond of Ala273. The dipole–dipole interaction is stabilized by altering the charge distribution along the DFG backbone, allowing or forcing the compact DFG-in state to unwind. (c) Geometric arrangement of inhibitors **4**–**9** and Ala273 in the experimentally determined dead-end complexes. Substituents able to induce the DFG flip (**6**–**9**) align linearly with the C_α–C_β bond of Ala273, whereas the C–F bonds of the DFG-in inhibitors **4** and **5** are positioned orthogonally.

5 did not invoke similar structural changes. Furthermore, proximity and net electronegativity alone do not explain these observations, as binding of the fluorinated substituents of **4** and **5** renders the DFG-in state unchanged. Superimposition of **7** onto the DFG-in state simulates the collision complex of halogenated inhibitors with the active site prior to the DFG flip (Figure 4a). Comparison with the dead-end complex indicates that the chlorine atom attracts the methyl group of Ala273, resulting in ~0.8 Å shorter distance and almost collinear alignment of the Phe-Cl and C_α-C_β bonds. The positional shift of Ala273 toward the inhibitor is only observed for the halogenated compounds **4**–**8** and nitrile derivative **9** (Supplementary Figures 3 and 4).

Halogen substituents are known for their abilities to significantly enhance the activity of small molecule inhibitors,[20] but the mechanism for the attraction of halocarbons to active site residues is not fully understood. C–X groups (X = F, Cl, Br) frequently display lipophilic characteristics, such as fitting into a hydrophobic pocket as observed for the fluorine substituent of **10** (Figure 3). Recent analyses of the PDB revealed a large number of halogenated ligands that appear to establish polar "halogen bonding" interactions with their target proteins.[21–23] Noncovalent halogen bonds are weaker than hydrogen bonding interactions and are typically established with polar acceptor groups in the form of perpendicular C–X···H or linear C–X···D bonds, in which D (electron donor) is a Lewis base.[24] We considered halogen bonding as a potential mechanism for our DFG-out inhibitors, taking into account the concept of the "sigma-hole",[25] which describes the positive electrostatic potential at the tip of the C-X bond due to the unevenly distributed partial charges around the halogen atom (Cl, Br, and I). C–X bonds therefore assume either electrophilic or nucleophilic characteristics, depending on the geometry of the halogen bond.[26,27] Halogen bonding is highly directional, with the C-X···D bond typically existing in a linear alignment (angles between 140° and 180°).[28–30] This implies that the strength of the sigma-hole halogen bond is directly related to the C-X···D alignment, with the strongest orbital overlap in the linear orientation and deviation from 180° resulting in a partial to total loss of effect. In the case of our DFG-out inhibitors, however, several experimental observations render halogen bonding interactions an unlikely cause for the DFG flip. First, the sigma-hole concept may be applicable to the chlorine and bromine substituents of **7** and **8** but not to the fluorine of **6**.[23] Second, the methyl group of Ala273 is a poor Lewis base/electron donor for an interaction of this nature. Third, halogen bonding interactions contribute to the binding potential of small molecules only moderately and have not been associated with conformational changes in proteins. The magnitude of the structural changes in Aurora A induced by inhibitors **6**–**8** therefore suggested a different mechanism of action involving electrostatic dipole–dipole interactions.

Induced-Dipole Forces Likely Cause the DFG To Unwind. The fundamental concept that polar molecules have the ability to polarize a second, nonpolar molecule[31] has been given much attention in molecular dynamics simulations to understand and predict the influence of electrostatic and van der Waals forces in proteins.[32–34] The asymmetric packing of the main chain amide dipoles in folded proteins results in overall positive electrostatic potential of all side chains, particularly for alanine.[35] The dipole moment and molecular orbital signature of L-alanine has been thoroughly analyzed,[36] and the polarizability of Ala273 in Aurora A may therefore play an important role in the mode of action of our inhibitors. The Phe–X bonds of **6**–**8** align with the C_α–C_β bond of Ala273, reminiscent of the attraction exerted by a permanent magnet on an iron rod (Figure 4b). In this mechanism, the electric dipole of the inhibitor induces a dipole in the polarizable C_α–C_β bond of Ala273. Establishment of this dipole–dipole interaction is relayed to the π-system of the amide bond, altering the charge distribution along the DFG backbone and allowing unrestrained rotation. As a consequence, the DFG unwinds and the activation loop adopts a potentially lower energy state. Such an unprecedented mechanism of action is difficult to prove, and

computational drug design has not probed the effect of exogenous electric dipoles on protein structure.[22]

To test the hypothesis of induced-dipole forces being responsible for the DFG flip and to rule out halogen bonding as a plausible mechanism, we introduced the strong dipolar and electron-withdrawing nitrile group.[37,38] As expected, compound **9** induced the same structural changes as inhibitors **6**−**8** (Figure 1), demonstrating that the DFG-in state of Aurora A is readily perturbed by dipoles able to align with Ala273. The distances between the substituents and the C_β atom of Ala273 range from 3.9 Å for the fluorine to as low as 3.0 Å for the nitrile substituent (Figure 4c). While the respective halocarbon bonds are positioned almost collinearly with the C_α−C_β bond of Ala273, accommodation of the longer nitrile group necessitates rotation of the A-ring out of the energetically favored position by ∼20°. Although slightly misaligned, the close proximity of the nitrile dipole to Ala273 induces the same conformational changes in the enzyme as the halogen substituents. However, steric repulsion exerted by Ala273 evidently causes strain in the inhibitor molecule explaining the decrease of binding potential for **9** (Table 1). It appears that the inhibitory efficacy of DFG-out inhibitors harboring electric dipoles depends on a precise geometry between the substituents and the flanking alanine residue. Although Ala273 is in close distance to inhibitors **4** and **5**, the dipoles introduced by the -CF_3 and -OCF_3 substituents lack the potential to induce the DFG flip. The C−F bonds are positioned almost orthogonal to the C_α−C_β bond, and steric repulsion prevents the proper alignment of the overall dipole along the Phe−CF_3 axis of **4** with Ala273 (∼ 150° angle and 4 Å distance).
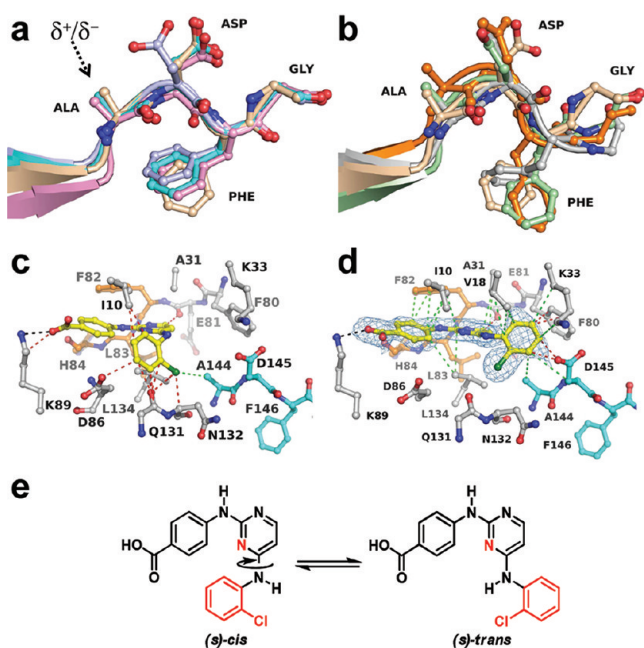
Implications for the Design of DFG-out Inhibitors of Other Kinases. The DFG-out inhibitors designed herein are among the most potent described for Aurora A and protein kinases in general. The ADFG sequence and the three-dimensional architecture of the DFG-in state are well-conserved among kinases for which structural information is available (Table 2, Figure 5a and b). It is conceivable that kinases with highest structural similarity to the DFG-in state of Aurora A respond similarly to the introduction of electric dipoles directed at the flanking alanine residue. The bisanilinopyrimidine scaffold of **1** proved to be advantageous for the design of DFG-out inhibitors of Aurora A, as it already binds with high affinity to the DFG-in state. However, slight variations in the ATP site may prevent proper positioning of this scaffold to other kinases. For example, compounds **1** and **7** are poor inhibitors of CDK2 with IC_{50} values of 11 and 15 μM, respectively. With the exception of CDK8,[39] CDKs are known only in the DFG-in state, despite the numerous inhibitor scaffolds that have been discovered. The conformation of the C-terminal DFG flank in CDK2 differs significantly from most kinases and probably contributes to stabilization of the DFG-in state. Modeling of the conformer of **7** (Aurora A) into the active site of CDK2 indicates substantial steric hindrance caused by the A-ring (Figure 5c). Co-crystal structures revealed that these inhibitors bind to CDK2 in the (*s*)-*trans* conformation as opposed to the (*s*)-*cis* conformation adopted in Aurora A (Figure 5d). As a result, the A-ring projects away from the DFG, preventing dipolar substituents from linear alignment with Ala273. Therefore, targeting the DFG of other kinases by induced-dipole forces initially requires the identification of candidate scaffolds that satisfy the geometric framework for efficient interaction with the N-terminal flank.

Table 2. Structural Comparison of the DFG-in States of Selected Kinases Harboring an ADFG Sequence

PDB ID	overall identity/similarity (%)[a]	kinase	rmsd (Å)[b]
2HK5	22.3/41.1	HCK	0.2
2DQ7	23.8/40.9	Fyn	0.2
1QPC	23.7/39.0	LCK	0.2
2ZV7	23.8/40.2	Lyn	0.2
3KF4	24.8/42.6	ABL1	0.3
2EU9	19.9/36.5	CLK3	0.3
3COK	35.1/56.2	PLK4	0.3
2XIK	30.3/49.0	STK25	0.3
2J7T	28.3/46.9	STK10	0.3
3A7F	28.6/48.1	STK24	0.3
3COM	26.8/49.7	STK4	0.3
2QLU	21.7/41.5	ACTR-IIB	0.3
2J51	28.5/49.3	hSLK	0.3
3S9S	22.8/39.9	LIMK1	0.3
3LXL	24.6/42.4	JAK3	0.3
2BDJ	22.9/40.5	Src	0.3
1XJD	30.8/49.3	PKC theta	0.4
2VD5	30.8/48.4	DMPK	0.4
2ETR	30.2/48.2	ROCK 1	0.5
2VZ6	31.3/48.1	CaMK2A	0.5
3DAK	25.9/41.3	OSR1	1.0
3PXR	26.4/44.4	CDK2	1.0
3FE3	31.2/51.5	MAPK3	1.0
3LMG	20.8/39.1	erbB-3	1.0
3KY2	25.4/42.2	FGFR1	1.1
3L8P	25.2/40.2	Tie-2	1.2
3PLS	21.3/35.4	RON	1.2
3BRB	22.9/36.7	MER	1.3
1BLX	24.3/41.0	CDK6	1.3
3F66	21.1/36.0	c-Met	1.4

[a]Computed with EMBOSS Needle (http://www.ebi.ac.uk/Tools/psa/emboss_needle/) against the kinase domain of human Aurora A. [b]rmsd = root-mean-square deviation of the main chain atoms upon superposition with the ADFG of Aurora A in complex with **1** (computed with Superpose from the CCP4 program suite).

Conclusions. Starting with a typical DFG-in inhibitor scaffold of Aurora A, we determined a series of co-crystal structures with monosubstituted analogues of parent compound **1** and used this information to design highly potent DFG-out inhibitors. The data suggest an unprecedented mechanism of action to induce the DFG flip in Aurora A, and possibly other kinases as well, by induced-dipole forces. The vast majority of kinase inhibitors are so-called Type I inhibitors such as compounds **1**−**5**, which simply compete with ATP for binding to the open DFG-in state. The underlying mechanism by which small molecules induce the DFG flip is not understood, and experimental data are limited to a few well-studied cases such as Abl, p38-MAP, and MEK1.[40,41] For these kinases, potent and selective Type II (partially allosteric) and Type III (fully allosteric) inhibitors have been designed, which act by occupying a pocket adjacent to the ATP site.[42−44] Although the here designed inhibitors **6**−**11** are purely Type I, they induce and stabilize the DFG-out state with drastic consequences for the overall structure of the enzyme. These findings offer new opportunities in the rational design of DFG-out inhibitors of various kinases, by equipping suitable DFG-in inhibitor scaffolds with electric dipoles directed at the N-terminal flank.

Figure 5. Implications for the design of DFG-out inhibitors of other kinases. (a) The ADFG-in states of Aurora A (wheat), ABL1 (blue), Rock1 (pink), and LCK (cyan) are highly similar, indicating that exogenous dipoles directed at the alanine residue may induce similar structural changes in these kinases. (b) CDK2 (green), MAPK3 (orange), and MER (gray) adopt a different conformation in the C-terminal flank and therefore may respond to exogenous dipoles differently. The rmsd values for the ADFG-in state of various kinases with respect to Aurora A are shown in Table 2. (c) The conformation of **7** bound to the active site of Aurora A is incompatible for efficient binding with CDK2. The model was generated by superimposition of the complexes of Aurora-**7** and CDK2-**7**. (d) The co-crystal structure of CDK2 in complex with **7** reveals that the bisanilinopyrimidine scaffold adopts an (s)-trans conformation (defined as the position of the groups colored red across the C–N bond), the A-ring pointing away from the DFG. (e) The (s)-cis and (s)-trans conformation of **7** found in Aurora A and CDK2, respectively. The $2F_o - F_c$ electron density around the inhibitor in panel d is contoured at 1 σ. Potential hydrogen bonding, van der Waals interactions, and steric clashes are indicated as black, green, and red dotted lines, respectively. The structure of CDK2 with **1** is shown in Supplementary Figure 7.

■ METHODS

Reagents and Compounds. Reagents and compounds for biochemical and crystallization experiments were purchased from Sigma-Aldrich and Hampton Research unless otherwise indicated. The peptide substrate for activity assays was synthesized in the Moffitt Cancer Center Proteomics Core, and the Aurora inhibitor VX680 was from LC laboratories. The synthesis of inhibitors **1−11** is described elsewhere (Lawrence *et al.*, submitted). During protein purification, the protein concentration was determined using the Coomassie reagent from BioRad with bovine serum albumin as a standard. The concentration of crystallization grade proteins was determined by A280 molar absorbance using a nanodrop ND-1000 spectrophotometer (Nanodrop Technologies). Nonlinear regression analysis was performed using SigmaPlot (Systat Software).

Cloning and Expression. The gene coding for the human Aurora A kinase domain comprising residues 123−390 was synthesized by Geneart and subcloned into a modified pET28 plasmid to provide fusion with cleavable hexahistidine-tagged maltose binding protein (MBP). The protein was overexpressed in *E. coli* Tuner (DE3) cells at 16 °C.

Protein Purification. The enzyme was purified by FPLC using Ni^{2+}-affinity chromatography (GE Healthcare) in 50 mM phosphate

(pH 7.2) and 300 mM NaCl with a linear gradient of 10−250 mM imidazole, followed by overnight digestion with PreScission protease at 4 °C. The protein was exchanged into 50 mM MES (pH 6.5) and 1 mM DTT by rapid gel filtration, and the cleaved Aurora A construct and His_6-MBP proteins were separated using a SP Sepharose Fast Flow ion exchange column (GE Healthcare), eluted with a 0−500 mM NaCl linear gradient. The pooled eluate was then concentrated and loaded onto a HiLoad Prep grade 26/60 Superdex 200 column (GE Healthcare) equilibrated with 50 mM HEPES (pH 7.4), 100 mM NaCl, and 1 mM DTT. The resulting eluate yielded crystallization-grade monomeric enzyme.

Enzyme Activity Assay. The synthetic peptide LRRASLG served as a substrate for Aurora A. Formation of ADP from ATP was quantified using a coupled enzyme assay (DiscoverX) in which a fluorescent resorufin dye is generated from the interaction of ADP with hydrogen peroxide and 10-acetyl-3,7-dihydroxy-phenoxazine (excitation and emission wavelengths of 540 and 590 nm, respectively). Reactions were carried out at RT in 15 mM HEPES buffer (pH 7.4) containing 20 mM NaCl, 1 mM EGTA, 0.02% Tween 20, 10 mM $MgCl_2$, 5% (v/v) DMSO, and 2.3 nM Aurora A. Inhibitor was added to the mixture, and the reaction was initiated by the addition of 75 μM ATP and 2 mM peptide substrate. All kinetic assays were performed in 384-well plates using a Wallac Envision 2102 plate reader (Perkin-Elmer). IC_{50} values for were obtained by fitting the data to eq 1:

$$A = \cfrac{1}{1 + \left(\cfrac{[I]}{IC_{50}} \right)^n}$$

(1)

where A is the remaining activity, $[I]$ is the concentration of the inhibitor, and n is the Hill slope coefficient. CDK2 IC_{50} values were measured using the same assay as described.[45] The dose−response curves are shown in Supplementary Figure 1.

Isothermal Titration Calorimetry (ITC). The binding of inhibitors to Aurora A kinase was analyzed with a MicroCal iTC200 titration calorimeter (GE Healthcare). The protein was exchanged into 100 mM Na/K phosphate (pH 7.4) *via* PD-10 columns (GE Healthcare). A total of 18 aliquots (2.2 μL each) of the protein solution (125 μM) were injected into 200 μL of the inhibitor solution (10 μM) at 25 °C. The ITC cell mixture was constantly stirred at 1000 rpm and recorded for 120 s between injections. Heat generation due to dilution (blank) was determined in a separate experiment by diluting protein into buffer. The corrected heat values were fitted using a nonlinear least-squares curve-fitting algorithm (Microcal Origin 7.0) to obtain the stoichiometry (n), binding constant (K_a, K_d), and change in enthalpy of the enzyme−ligand interaction (ΔH). The ITC graphs are shown in the Supplementary Figure 2.

Protein Crystallography. Aurora A was exchanged into 50 mM phosphate buffer (pH 7.4) including 1 mM DTT *via* PD-10 columns and was concentrated to 20 mg mL^{-1} using Amicon Ultra-4 10K centrifugal devices (Millipore). Aurora A crystals were grown using sitting drop vapor diffusion at 18 °C from a 1:1 volume ratio of Aurora A and reservoir solution (200 mM sodium tartrate/20% (v/v) poly(ethylene glycol) 3350 for the DFG-in inhibitors or 10% (v/v) Tacsimate/20% (v/v) poly(ethylene glycol) 3350 for the DFG-out inhibitors) with a final inhibitor concentration of 1 mM. Crystals appeared after 2 days and were allowed to grow for another 2 days. For data collection, crystals were harvested in a cryoprotectant mixture consisting of the respective reservoir composition including 1 mM inhibitor, 50 mM phosphate pH (7.4), and 25% (v/v) ethylene glycol. Diffraction data were recorded at −180 °C in the Moffitt Cancer Center Chemical Biology Core using Cu Kα X-rays generated by a Rigaku Micro-Max 007-HF X-ray generator, focused by mirror optics and equipped with a Rigaku CCD Saturn 944 system on single crystals frozen in liquid N_2. Data were reduced with XDS.[46] The "DFG-in" crystals belonged to the $P6_122$ space group, containing one monomer in the asymmetric unit. The "DFG-out" crystals belonged to space group $P3_2$ with two monomers in the asymmetric unit. The structures were determined by molecular replacement using MOLREP (CCP4)[47]

and PDB entry 3FDN as the search model. PHENIX[48] was employed for refinement (minimization and simulated annealing), and model building was performed using Coot.[49] Figures were drawn with PyMol (Schrödinger, LLC). CDK2 was co-crystallized with compounds **1** and **7** using previously established conditions,[45] and the structures were determined accordingly. Data and refinement statistics are shown in the Supplementary Table 1, along with the $F_o - F_c$ electron density maps from refinement cycles omitting the respective ligand (Supplementary Figures 5−7).

■ ASSOCIATED CONTENT

Ⓢ Supporting Information

Additional data analysis. This material is available free of charge *via* the Internet at http://pubs.acs.org.

Accession Codes

The atomic coordinates and structure factors for Aurora A in complex with compounds **1** and **3−11**, and CDK2 in complex with compounds **1** and **7**, have been deposited under accession numbers 3UO5, 3UO4, 3UOD, 3UP2, 3UNZ, 3UO6, 3UOH, 3UOJ, 3UOK, 3UOL, 3UNJ and 3UNK, respectively. The crystal structure of Aurora A with **2** has been deposited separately (Lawrence *et al.*, submitted) under code 3UP7.

■ AUTHOR INFORMATION

Corresponding Author
*E-mail: ernst.schonbrunn@moffitt.org.

Notes
The authors declare no competing financial interest.

■ ACKNOWLEDGMENTS

■ REFERENCES

(1) Dar, A. C., and Shokat, K. M. (2011) The evolution of protein kinase inhibitors from antagonists to agonists of cellular signaling. *Ann. Rev. Biochem. 80*, 769−795.

(2) Carmena, M., and Earnshaw, W. C. (2003) The cellular geography of aurora kinases. *Nat. Rev. Mol. Cell. Biol. 4*, 842−854.

(3) Marumoto, T., Zhang, D., and Saya, H. (2005) Aurora-A—a guardian of poles. *Nat. Rev. Cancer 5*, 42−50.

(4) Xu, X., Wang, X., Xiao, Z., Li, Y., and Wang, Y. (2011) Two TPX2-dependent switches control the activity of Aurora A. *PLoS One 6*, e16757.

(5) Becker, M., Stolz, A., Ertych, N., and Bastians, H. (2010) Centromere localization of INCENP-Aurora B is sufficient to support spindle checkpoint function. *Cell Cycle 9*, 1360−1372.

(6) Gritsko, T. M., Coppola, D., Paciga, J. E., Yang, L., Sun, M., Shelley, S. A., Fiorica, J. V., Nicosia, S. V., and Cheng, J. Q. (2003) Activation and overexpression of centrosome kinase BTAK/Aurora-A in human ovarian cancer. *Clin. Cancer Res. 9*, 1420−1426.

(7) Keen, N., and Taylor, S. (2004) Aurora-kinase inhibitors as anticancer agents. *Nat. Rev. Cancer 4*, 927−936.

(8) Harrington, E. A., Bebbington, D., Moore, J., Rasmussen, R. K., Ajose-Adeogun, A. O., Nakayama, T., Graham, J. A., Demur, C., Hercend, T., Diu-Hercend, A., Su, M., Golec, J. M., and Miller, K. M. (2004) VX-680, a potent and selective small-molecule inhibitor of the Aurora kinases, suppresses tumor growth in vivo. *Nat. Med. 10*, 262−267.

(9) Green, M. R., Woolery, J. E., and Mahadevan, D. (2011) Update on Aurora kinase targeted therapeutics in oncology. *Expert Opin. Drug Discovery 6*, 291−307.

(10) Howard, S., Berdini, V., Boulstridge, J. A., Carr, M. G., Cross, D. M., Curry, J., Devine, L. A., Early, T. R., Fazal, L., Gill, A. L., Heathcote, M., Maman, S., Matthews, J. E., McMenamin, R. L., Navarro, E. F., O'Brien, M. A., O'Reilly, M., Rees, D. C., Reule, M., Tisi, D., Williams, G., Vinkovic, M., and Wyatt, P. G. (2009) Fragment-based discovery of the pyrazol-4-yl urea (AT9283), a multitargeted kinase inhibitor with potent aurora kinase activity. *J. Med. Chem. 52*, 379−388.

(11) Gorgun, G., Calabrese, E., Hideshima, T., Ecsedy, J., Perrone, G., Mani, M., Ikeda, H., Bianchi, G., Hu, Y., Cirstea, D., Santo, L., Tai, Y.-T., Nahar, S., Zheng, M., Bandi, M., Carrasco, R. D., Raje, N., Munshi, N., Richardson, P., and Anderson, K. C. (2010) A novel Aurora-A kinase inhibitor MLN8237 induces cytotoxicity and cell-cycle arrest in multiple myeloma. *Blood 115*, 5202−5213.

(12) Nagar, B., Bornmann, W. G., Pellicena, P., Schindler, T., Veach, D. R., Miller, W. T., Clarkson, B., and Kuriyan, J. (2002) Crystal structures of the kinase domain of c-Abl in complex with the small molecule inhibitors PD173955 and imatinib (STI-571). *Cancer Res. 62*, 4236−4243.

(13) Seeliger, M. A., Ranjitkar, P., Kasap, C., Shan, Y., Shaw, D. E., Shah, N. P., Kuriyan, J., and Maly, D. J. (2009) Equally potent inhibition of c-Src and Abl by compounds that recognize inactive kinase conformations. *Cancer Res. 69*, 2384−2392.

(14) Angell, R. M., Angell, T. D., Bamborough, P., Bamford, M. J., Chung, C. W., Cockerill, S. G., Flack, S. S., Jones, K. L., Laine, D. I, Longstaff, T., Ludbrook, S., Pearson, R., Smith, K. J., Smee, P. A., Somers, D. O., and Walker, A. L. (2008) Biphenyl amide p38 kinase inhibitors 4: DFG-in and DFG-out binding modes. *Bioorg. Med. Chem. Lett. 18*, 4433−4437.

(15) Kuglstatter, A., Ghate, M., Tsing, S., Villasenor, A. G., Shaw, D., Barnett, J. W., and Browner, M. F. (2010) X-ray crystal structure of JNK2 complexed with the p38alpha inhibitor BIRB796: insights into the rational design of DFG-out binding MAP kinase inhibitors. *Bioorg. Med. Chem. Lett. 20*, 5217−5220.

(16) Solanki, S., Innocenti, P., Mas-Droux, C., Boxall, K., Barillari, C., van Montfort, R. L., Aherne, G. W., Bayliss, R., and Hoelder, S. (2011) Benzimidazole inhibitors induce a DFG-out conformation of never in mitosis gene A-related kinase 2 (Nek2) without binding to the back pocket and reveal a nonlinear structure-activity relationship. *J. Med. Chem. 54*, 1626−1639.

(17) Choi, Y., Syeda, F., Walker, J. R., Finerty, P. J. Jr., Cuerrier, D., Wojciechowski, A., Liu, Q., Dhe-Paganon, S., and Gray, N. S. (2009) Discovery and structural analysis of Eph receptor tyrosine kinase inhibitors. *Bioorg. Med. Chem. Lett. 19*, 4467−4470.

(18) Dietrich, J., Hulme, C., and Hurley, L. H. (2010) The design, synthesis, and evaluation of 8 hybrid DFG-out allosteric kinase inhibitors: a structural analysis of the binding interactions of Gleevec, Nexavar, and BIRB-796. *Bioorg. Med. Chem. 18*, 5738−5748.

(19) Filomia, F., De Rienzo, F., and Menziani, M. C. (2010) Insights into MAPK p38alpha DFG flip mechanism by accelerated molecular dynamics. *Bioorg. Med. Chem. 18*, 6805−6812.

(20) Muller, K., Faeh, C., and Diederich, F. (2007) Fluorine in pharmaceuticals: looking beyond intuition. *Science 317*, 1881−1886.

(21) Lu, Y., Shi, T., Wang, Y., Yang, H., Yan, X., Luo, X., Jiang, H., and Zhu, W. (2009) Halogen bonding—a novel interaction for rational drug design? *J. Med. Chem. 52*, 2854−2862.

(22) Lu, Y., Wang, Y., Xu, Z., Yan, X., Luo, X., Jiang, H., and Zhu, W. (2009) C-X...H contacts in biomolecular systems: how they contribute to protein-ligand binding affinity. *J. Phys. Chem. B 113*, 12615−12621.

(23) Parisini, E., Metrangolo, P., Pilati, T., Resnati, G., and Terraneo, G. (2011) Halogen bonding in halocarbon-protein complexes: a structural survey. *Chem. Soc. Rev. 40*, 2267−2278.

(24) Metrangolo, P., Resnati, G., Arman, H. D. (2008) *Halogen Bonding: Fundamentals and Applications*, Springer, New York.

(25) Auffinger, P., Hays, F. A., Westhof, E., and Ho, P. S. (2004) Halogen bonds in biological molecules. *Proc. Natl. Acad. Sci. U.S.A. 101*, 16789−16794.

(26) Politzer, P., Lane, P., Concha, M. C., Ma, Y., and Murray, J. S. (2007) An overview of halogen bonding. *J. Mol. Model. 13*, 305−311.

(27) Murray, J. S., Lane, P., and Politzer, P. (2009) Expansion of the sigma-hole concept. *J. Mol. Model. 15*, 723−729.

(28) Metrangolo, P., and Resnati, G. (2001) Halogen bonding: a paradigm in supramolecular chemistry. *Chemistry 7*, 2511−2519.

(29) Metrangolo, P., Meyer, F., Pilati, T., Resnati, G., and Terraneo, G. (2008) Halogen bonding in supramolecular chemistry. *Angew. Chem., Int. Ed. 47*, 6114−6127.

(30) Politzer, P., Murray, J. S., and Clark, T. (2010) Halogen bonding: an electrostatically-driven highly directional noncovalent interaction. *Phys. Chem. Chem. Phys. 12*, 7748−7757.

(31) Atkins, P. W. (1978) *Physical Chemistry*, Vol. *1*, 1st ed., Oxford University Press, Oxford.

(32) Neves-Petersen, M. T., and Petersen, S. B. (2003) Protein electrostatics: a review of the equations and methods used to model electrostatic equations in biomolecules--applications in biotechnology. *Biotechnol. Annu. Rev. 9*, 315−395.

(33) Stork, M., and Tavan, P. (2007) Electrostatics of proteins in dielectric solvent continua. II. First applications in molecular dynamics simulations. *J. Chem. Phys. 126*, 165106.

(34) Nakamura, H. (1996) Roles of electrostatic interaction in proteins. *Q. Rev. Biophys. 29*, 1−90.

(35) Gunner, M. R., Saleh, M. A., Cross, E., ud-Doula, A., and Wise, M. (2000) Backbone dipoles generate positive potentials in all proteins: origins and implications of the effect. *Biophys. J. 78*, 1126−1144.

(36) Falzon, C. T., Wang, F., and Pang, W. (2006) Orbital signatures of methyl in L-alanine. *J. Phys. Chem. B 110*, 9713−9719.

(37) Jones, L. H., Summerhill, N. W., Swain, N. A., and Mills, J. E. (2010) Aromatic chloride to nitrile transformation: medicinal and synthetic chemistry. *MedChemComm 1*, 309−318.

(38) Fleming, F. F., Yao, L., Ravikumar, P. C., Funk, L., and Shook, B. C. (2010) Nitrile-containing pharmaceuticals: efficacious roles of the nitrile pharmacophore. *J. Med. Chem. 53*, 7902−7917.

(39) Schneider, E. V., Bottcher, J., Blaesse, M., Neumann, L., Huber, R., and Maskos, K. (2011) The structure of CDK8/CycC implicates specificity in the CDK/cyclin family and reveals interaction with a deep pocket binder. *J. Mol. Biol. 412*, 251−266.

(40) Schindler, T., Bornmann, W., Pellicena, P., Miller, W. T., Clarkson, B., and Kuriyan, J. (2000) Structural mechanism for STI-571 inhibition of abelson tyrosine kinase. *Science 289*, 1938−1942.

(41) Pargellis, C., Tong, L., Churchill, L., Cirillo, P. F., Gilmore, T., Graham, A. G., Grob, P. M., Hickey, E. R., Moss, N., Pav, S., and Regan, J. (2002) Inhibition of p38 MAP kinase by utilizing a novel allosteric binding site. *Nat. Struct. Biol. 9*, 268−272.

(42) Zhang, J., Adrian, F. J., Jahnke, W., Cowan-Jacob, S. W., Li, A. G., Iacob, R. E., Sim, T., Powers, J., Dierks, C., Sun, F., Guo, G. R., Ding, Q., Okram, B., Choi, Y., Wojciechowski, A., Deng, X., Liu, G., Fendrich, G., Strauss, A., Vajpai, N., Grzesiek, S., Tuntland, T., Liu, Y., Bursulaya, B., Azam, M., Manley, P. W., Engen, J. R., Daley, G. Q., Warmuth, M., and Gray, N. S. (2010) Targeting Bcr-Abl by combining allosteric with ATP-binding-site inhibitors. *Nature 463*, 501−506.

(43) Comess, K. M., Sun, C., Abad-Zapatero, C., Goedken, E. R., Gum, R. J., Borhani, D. W., Argiriadi, M., Groebe, D. R., Jia, Y., Clampit, J. E., Haasch, D. L., Smith, H. T., Wang, S., Song, D., Coen, M. L., Cloutier, T. E., Tang, H., Cheng, X., Quinn, C., Liu, B., Xin, Z., Liu, G., Fry, E. H., Stoll, V., Ng, T. I., Banach, D., Marcotte, D., Burns, D. J., Calderwood, D. J., and Hajduk, P. J. (2011) Discovery and characterization of non-ATP site inhibitors of the mitogen activated protein (MAP) kinases. *ACS Chem. Biol. 6*, 234−244.

(44) Dong, Q., Dougan, D. R., Gong, X., Halkowycz, P., Jin, B., Kanouni, T., O'Connell, S. M., Scorah, N., Shi, L., Wallace, M. B., and Zhou, F. (2011) Discovery of TAK-733, a potent and selective MEK allosteric site inhibitor for the treatment of cancer. *Bioorg. Med. Chem. Lett. 21*, 1315−1319.

(45) Betzi, S., Alam, R., Martin, M., Lubbers, D. J., Han, H., Jakkaraj, S. R., Georg, G. I., and Schonbrunn, E. (2011) Discovery of a potential allosteric ligand binding site in CDK2. *ACS Chem. Biol. 6*, 492−501.

(46) Kabsch, W. (1993) Automatic processing of rotation diffraction data from crystals of initially unknown symmetry and cell constants. *J. Appl. Crystallogr. 26*, 795−800.

(47) (1994) The CCP4 suite: programs for protein crystallography, *Acta Crystallogr. Sect. D: Biol. Crystallogr. 50*, 760−763.

(48) Adams, P. D., Afonine, P. V., Bunkoczi, G., Chen, V. B., Davis, I. W., Echols, N., Headd, J. J., Hung, L. W., Kapral, G. J., Grosse-Kunstleve, R. W., McCoy, A. J., Moriarty, N. W., Oeffner, R., Read, R. J., Richardson, D. C., Richardson, J. S., Terwilliger, T. C., and Zwart, P. H. (2010) PHENIX: a comprehensive Python-based system for macromolecular structure solution. *Acta Crystallogr., Sect. D: Biol. Crystallogr. 66*, 213−221.

(49) Emsley, P., and Cowtan, K. (2004) Coot: model-building tools for molecular graphics. *Acta Crystallogr., Sect. D: Biol. Crystallogr. 60*, 2126−2132.